RESEARCH PAPER

PCCP
www.rsc.org/pccp

Recombination of benzyl radicals: dependence on the bath gas, temperature, and pressure

Klaus Luther, Kawon Oum,* Kentaro Sekiguchi and Jürgen Troe

Institut für Physikalische Chemie, Universität Göttingen, Tammannstraße 6 D-37077, Göttingen, Germany. E-mail: koum@gwdg.de; Fax: + 49 551 393150; Tel: + 49 551 3912598

Received 11th May 2004, Accepted 7th July 2004
First published as on Advance Article on the web 21st July 2004

The combination reaction $C_6H_5CH_2 + C_6H_5CH_2$ (+M) → $C_{14}H_{14}$ (+M) was studied over the pressure range 0.03–900 bar and the temperature range 250–400 K. Helium, argon, xenon, N_2 and CO_2 were employed as bath gases. Benzyl radicals were generated by H abstraction from toluene by Cl atoms formed via laser photolysis of Cl_2 at 308 nm. Benzyl radicals were monitored by time-resolved transient UV absorption at 253 nm. The observed combination rates were pressure independent over the range 0.04–0.45 bar in CO_2 and 0.03–5 bar in argon which identifies a limiting "high-pressure" value of rate constant within the energy-transfer mechanism, $k_\infty^{ET}(T) = (4.1 \pm 0.3) \times 10^{-11}\ (T/300\ K)^{-0.23}$ cm^3 molecule^{-1} s^{-1}. Although the reaction has clearly reached the "high-pressure limit" (k_∞^{ET}) at pressures below 1 bar, a further increase of the rate constants was observed when the pressure of the bath gas was raised above ~5 bar. At much higher pressures finally the rate constants decrease when diffusion-controlled kinetics takes over. The degree of enhancement of the combination rates beyond the "high-pressure limit" was found to depend on the bath gas, increasing in the order He < N_2 ≈ Ar < CO_2. The enhancement was most prominent at low temperatures. Measurements of transient UV absorption spectra of benzyl radicals, over the pressure range 5–30 bar of CO_2 at 300 K, confirmed that an only small pressure-dependent solvatochromic shift of benzyl radicals cannot be responsible for the observation of enhanced rate constants. Instead, the results clearly point toward a significant effect of van der Waals clustering, *i.e.* of "radical-complex" formation, on the combination reaction kinetics in the gas–liquid transition range. An analysis in terms of statistical adiabatic channel/classical trajectory calculation (SACM/CT) appears to provide a consistent description.

1. Introduction

Intermolecular interactions between solute and solvent molecules are of great interest for an understanding of kinetic and dynamic properties of radical reactions in the gas–liquid transition region.[1–3] Studies of the pressure and temperature dependence of radical combination rate constants in this range can help to identify contributions of the corresponding van der Waals complexes to rate constants.[4,5] Recently we have observed an unexpected enhancement of combination rates of polyatomic radicals, such as CCl_3[6] or benzyl[7] at pressures higher than those where the "high-pressure limit" of the standard energy-transfer (ET) mechanism is established. The reason for such a pressure- and temperature-dependent increase of combination rate constants has been not yet completely understood. However, currently available information suggests that interactions between radicals and solvent molecules may be responsible for the phenomenon, which then can be described in terms of a radical-complex (RC) mechanism and/or the density dependence of electronic quenching.[6] More experimental studies appear necessary to separate and clarify, qualitatively and quantitatively, the influence of radical-solvent molecule interactions on the radical combination kinetics in the gas–liquid transition region. In the present article, we report new studies of the combination reaction of benzyl radicals over the wide pressure range 0.03–900 bar and the temperature range 250–400 K in the bath gases (M) helium, argon, xenon, N_2, and CO_2:

$$C_6H_5CH_2 + C_6H_5CH_2\ (+M) \rightarrow C_{14}H_{14}\ (+M)\ k_1 \qquad (1)$$

A number of kinetic studies of reaction (1) have been reported in the gas phase,[8–10] in liquid solutions,[11] and recently in the medium density region of supercritical fluids.[7,12] On the one hand, our result in the normal gas phase of $k_{1,\infty}^{ET}$, "high-pressure limit" of the combination, $(4.1 \pm 0.3) \times 10^{-11}$ cm^3 molecule^{-1} s^{-1},[7] is comparable to two previous direct experimental measurements.[9,10] On the other hand, at the highest pressure of our work, reaction (1) is diffusion-controlled and our rate constants k_1 are equivalent to the values from the work of Claridge and Fischer[11] in the liquid solution. In the medium density region, we have observed a rapid increase of reaction rates at elevated pressures beyond the normal "high-pressure limit" before the diffusion control sets in. The interpretation of our experimental observations in terms of a possible contribution of the radical-complex mechanism is the central topic of the present article. In continuation of our earlier Communication,[7] in the following we present a full report of our work.

2. Experimental section

2.1. Time-resolved absorption measurements in the UV

Our high-pressure set up has been described in detail before,[13–15] and only the main features are given here. In brief, our experiment was carried out in a high-pressure optical flow cell which can be cooled or heated over the temperature range 200–400 K at pressures of 1–1000 bar. Benzyl radicals were generated by the laser photolysis of Cl_2 at 308 nm using an excimer laser (Lambda Physik, model COMPEX), and the subsequent fast bimolecular reaction of chlorine atoms with an excess amount of toluene ($C_6H_5CH_3$):

$$Cl_2 + h\nu\ (308\ nm) \rightarrow 2\ Cl \qquad (2)$$

$$Cl + C_6H_5CH_3 \rightarrow C_6H_5CH_2 + HCl \qquad (3)$$

DOI: 10.1039/b407074g

Mixtures of Cl_2, toluene, and the bath gas were compressed in an oil-free diaphragm compressor (Nova Swiss), and then flowed through the high-pressure cell (path length of 10 cm and optical diameter of 0.9 cm). For experiments <1 bar, a flow cell made of glass was used (path length of 52 cm and optical diameter of 3 cm). Flow rates were controlled by flow meters (Tylan, model FM361 and FM362) at rates such that reagents and products were removed from the observation volume between the laser pulses. Total pressures were measured with high-pressure meters (Burster, model 8201). Two platinum resistance thermometers were directly attached to the front and back of the cell to measure the temperature.

The progress of reaction (1) was monitored by recording the absorption signal of benzyl radicals at 253 nm on time scales of μs to ms. The light source for the absorption measurements was a high-intensity Hg–Xe lamp (Ushio, model UXM-200 H, 200W). At 253 nm, the absorption of benzyl radicals dominates over contributions from other species involved ($\sigma_{benzyl} = 1.3 \times 10^{-16}$ cm^2 molecule^{-1}).[16] The absorption signal was detected by a standard prism-monochromator (Zeiss, model MM3) and photomultiplier (RCA, 1P28A) arrangement with a bandwidth of 2 nm, and recorded using a digital storage oscilloscope (LeCroy, band width 200 MHz). Typically several hundred shots were averaged. The bath gases of helium, argon, xenon, N_2, and CO_2 were of a purity higher than 99.998%. Impurities in the bath gases, especially oxygen, were carefully removed by a series of gas cleaning adsorbers (Messer-Griesheim, model Oxisorb, and Alltech, model Oxytrap) and dust filters. All chemicals were purified in a pump–thaw–freeze cycle prior to use.

2.2. Transient absorption spectra

Prior to the analysis of the kinetics, it was necessary to check the pressure dependence of the absorption of benzyl radicals. In addition, possible contributions to the absorption signals from other reactants, intermediates, and products (for example, dibenzyl or benzyl chloride) over the observation wavelength range were investigated. It turned out that benzyl absortpion was predominant over the wavelength range 240–270 nm and times up to a few ms.

Pressure-dependent transient spectra of benzyl radicals were recorded at room temperature in a high-pressure flow cell closed by two quartz windows (path length of 29.5 cm and optical diameter of 0.9 cm). A Jobin-Yvon-Spex type of spectrograph (model SPEX 270M) with a holographic grating (1200 or 2400 g mm^{-1}, blazed at 500 nm) and a 384 × 576 pixel ICCD camera (LaVison, model FlameStar IIF) served as the detection system (wavelength range of 190–850 nm). The highest resolution of the spectrograph (0.096 nm) was determined by an entrance slit width of 12 μm. The minimum gating time was 1 ns. A high-pressure xenon arc lamp (Osram, model XBO 150W/1) was used as the light source. A set of lenses focused the light beam as it emerged from the highcell on to the entrance slit of the spectrograph. The 308 nm-excimer laser beam (Lambda Physik, model EMG 101MSC) and the light of the Xe lamp were directed collinearly through the highcell, *via* a set of laser mirrors (Laseroptik, high reflectance at 308 nm and high transmittance at 253 nm, 45°) in a counter-propagating arrangement. A laser power meter recorded the laser energy behind the high-pressure cell. A low-pressure mercury lamp (ORIEL, model 65130, 22–44 W) was used to calibrate the wavelength of the spectrum before the measurement. A pulse/delay generator (Stanford Research Systems, model DG535) was interfaced with the laser controlling system and the data acquisition system of the ICCD camera. Spectral analysis software (LaVision, DaVis version 6.0) was used for post-processing the measured spectra. Prior to obtaining the transient spectrum of benzyl radicals, a reference spectrum was measured without the laser beam at the same experimental conditions. Several hundred spectra were usually averaged.

3. Results

Fig. 1 shows typical absorption signals at 253 nm, recorded after the 308 nm-laser photolysis of Cl_2 in the presence of toluene and the bath gas CO_2 at 300 K. All absorption–time profiles showed clean second-order decays of the benzyl concentrations and agreed entirely with an assignment to reaction (1).

Reaction (3) is known to solely proceed through a fast H-atom abstraction channel ($k_3 = 6.1 \times 10^{-11}$ cm^3 molecule^{-1} s^{-1}) such that chlorine atoms rapidly, completely, and stoichiometrically lead to benzyl radicals.[17] The quantitative analysis of our experimental observation was carried out considering the major channel (1) and also accounting for other possible side reactions such as the recombination of chlorine atoms and the reaction between chlorine atoms and benzyl radicals:

$$Cl + Cl \rightarrow Cl_2 \quad (4)$$

$$C_6H_5CH_2 + Cl \rightarrow C_6H_5CH_2Cl \quad (5)$$

These two side reactions, however, turned out to be insignificant because the concentration of toluene was always present in significant excess. Residual absorptions from products like dibenzyl and benzyl chloride are also negligible due to their small absorption coefficients ($\sigma_{dibenzyl} \approx \sigma_{benzyl\ chloride} \approx 1 \times 10^{-19}$ cm^2 molecule^{-1})[18] compared to the strong absorption from benzyl radicals ($\sigma_{benzyl} = 1.3 \times 10^{-16}$ cm^2 molecule^{-1}).16 The residuals of the fits did not show any systematic deviations, giving additional support to the reported values of k_1. Typical concentrations used in our experiments were: $[Cl]_0$ (= $[benzyl]_0$) = (1 – 5) × 10^{13} molecule cm^{-3} and [toluene] = (0.7 – 7) × 10^{16} molecule cm^{-3}.

Several other precursor molecules for benzyl radicals were tested but found to be inadequate for our purpose. For example, benzyl iodide, ethylbenzene, and benzyl chloride also yield benzyl radicals in a direct photolytic step. However, subsequent side reactions of other photolytic products (such as halogen atoms or ethyl radicals) caused large difficulties of the analysis.

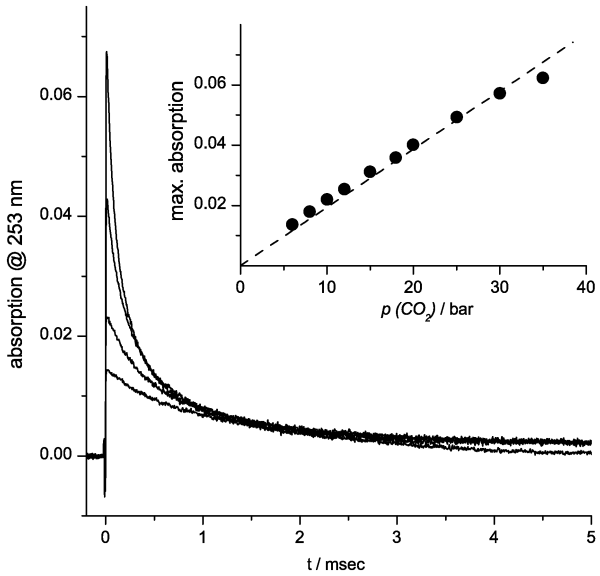

Fig. 1 Absorption signals at 253 nm, recorded after the photolysis at 308 nm of mixtures of Cl_2, toluene and CO_2 at $T = 300$ K. Main figure: time-profiles at different CO_2 pressures, from the top: 35, 20, 10, and 6 bar. The ratio of $[Cl_2]/[CO_2]$ was kept constant (1.3×10^{-5}). Inserted figure: (●) maximum absorption values as a function of the CO_2 bath gas pressure, (--) = linear fit.

Because of the second order kinetics of reaction (1), measured reaction rates are sensitive to the absolute initial concentration of benzyl radicals and therefore the value of their absorption coefficients. We checked if there was any influence of the pressure and temperature dependence of σ_{benzyl} on our evaluation of k_1. This was done by the following two methods. First, in Fig. 1, we kept a constant ratio of $[benzyl]_0/[CO_2]$ at different CO_2 pressures between 7 and 37 bar. The inset in Fig. 1 illustrates the maximum absorption values of benzyl radicals at time = 0 as a function of bath gas pressure. The linear relationship indicates that under our experimental conditions we could not see any unusual behaviour in our absorption signals due to solvent-induced spectral shifts or unusual changes of absolute absorption intensities. Second, we investigated the pressure dependence of the UV spectra of benzyl radicals in the bath gas CO_2 at 300 K; the results are shown in Fig. 2. CO_2 was chosen as the bath gas as it is expected to cause larger spectral shifts than the other bath gases employed. Our measured benzyl spectra recorded between 10 μs and 60 μs with a spectral resolution of 0.09 nm) were calibrated with the Hg line spectra at 253.4 nm, and compared with the spectrum of benzyl radical measured by Fay *et al.* after 193 nm photolysis of ethylbenzene in 5 mbar of argon (recorded between 1 μs and 3.2 μs).[16] We observed no significant spectral shift over the pressure range 5–30 bar. Maximum changes of the integrated absorption over the range (253 ± 1) nm at different CO_2 pressures in Fig. 2 corresponded to maximum errors of 5% in k_1, due to the small spectral shift of the spectrum illustrated in Fig. 2.

Our results on the pressure dependence of k_1 at 300 K are summarized in Table 1 and Fig. 3. The limiting "high-pressure" rate constant of the energy-transfer mechanism, which in this case corresponds to the value of k_1 at the lowest pressure investigated, was determined to be $k_{1,\infty}^{ET}$ (300 K) = (4.1 ± 0.3) × 10^{-11} cm^3 $molecule^{-1}$ s^{-1}, independent of the bath gas and considering all data points below 1 bar. At pressures above 1 bar, clear indications of a further increase of k_1 are recognized in Fig. 3. This pressure-induced enhancement of k_1 increases in the order He < N_2 ≈ Ar < CO_2, similar as observed in our recent study of combination reactions of CCl_3 radicals.[6] The finally observed decrease of the rate constants at pressures above 100 bar (in N_2 and argon), and above 60 bar (in CO_2), corresponds to a transition into the regime of diffusion-controlled kinetics such as expected at these pressures. A modest negative temperature dependence of $k_{1,\infty}^{ET}$ (*T*) was observed and measured over the temperature range 250–400 K. The results are summarized in Table 2 and compared in Fig. 4 with values from Lesclaux and co-workers in the temperature ranges 400–450 K[9] and 435–519 K.[10] In order to compare our results with the values from refs. 9 and 10 in Fig. 4, it was necessary to correct their rate constants using $\sigma_{benzyl}(T) \approx 1.3 \times 10^{-16}$ $(T/300\ K)^{-0.25}$ cm^2 $molecule^{-1}$. The temperature dependence of $\sigma_{benzyl}(T)$ was estimated from the work of Ikeda *et al.*[19] All measurements confirm that there is only a mild temperature dependence of $k_{1,\infty}^{ET}(T)$. The temperature dependence of $k_{1,\infty}^{ET}(T)$ over the temperature range 250–520 K, including results of refs. 9 and 10, could be expressed by:

$$k_{1,\infty}^{ET,experimental}(T) = (4.1 \pm 0.3) \times 10^{-11}(T/300\ K)^{-0.45}\ cm^3\ molecule^{-1}\ s^{-1} \quad (6)$$

The error limits in eqn. (6) represent the scatter of the data and an estimate of possible systematic errors.

The temperature dependence of the enhancement of k_1 over $k_{1,\infty}^{ET}$ was investigated in the bath gas CO_2 and the results are illustrated in Fig. 5 over the range 275–350 K. The enhancement of k_1 was found to be the more pronounced, the lower the temperature. We have also investigated the possibility of a heavy atom effect on the enhancement of k_1 which might be the consequence of electronic quenching effects. Using bath gas mixtures of argon and xenon, however, we found no notable increase of k_1 compared to measurements in pure argon when similar density conditions were compared (see Table 1(g) and 1(h)).

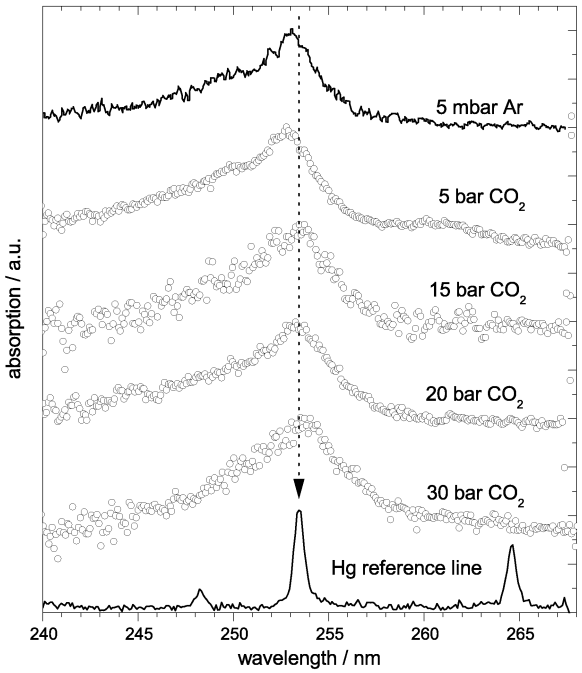

Fig. 2 Transient spectra of benzyl in the bath gas CO_2 over the range of 5–30 bar. (○): this work, delay time = 10 μs, gating time = 50 μs, and spectral resolution 0.09 nm; (— at the top of the figure): cold spectrum of benzyl radical in 5 mbar of Ar from ref. 16; (— at the bottom of the figure): Hg reference line; the arrow points at 253.4 nm.

4. Discussion

4.1. Experimental "high-pressure" rate constant, $k_{1,\infty}^{ET}(T)$

Reaction (1) has been previously studied in 1 bar of N_2 by Fenter *et al.*[9] in the temperature range 400–450 K and Boyd *et al.*[10] from 435 to 519 K. Their results of rate constant k_1 were obtained with the reported literature absorption cross-section σ_{benzyl} (253 nm, 300 K) = 1.1 × 10^{-16} cm^2 $molecule^{-1}$ by Ikeda *et al.*[19] and Markert and Pagsberg.[20] From this, Boyd *et al.* determined $k_{1,\infty}^{ET}$ to be (2.9 ± 0.3) × 10^{-11} cm^3 $molecule^{-1}$ s^{-1} with a total uncertainty of ~40%. Boyd *et al.* furthermore reduced the previous result of Fenter *et al.* from (4.6 ± 2.5) × 10^{-11} cm^3 $molecule^{-1}$ s^{-1} to (3.9 ± 1.9) × 10^{-11} cm^3 $molecule^{-1}$ s^{-1}, after they allowed for a temperature dependence of $\sigma_{benzyl}(T)$ recommended by Ikeda *et al.*[19] From a careful redetermination, Fay[16] has recently reported a slightly higher value of σ_{benzyl} = 1.3 × 10^{-16} cm^2 $molecule^{-1}$, obtained from a cold spectrum of benzyl radicals after relaxation to 300 K: We have used this value in our evaluation. Using the latter value of σ_{benzyl}, the results from refs. 9 and 10 agree with the present results as shown in Fig. 4.

However, our rate expression in eqn. (6) (both the absolute value and the temperature coefficient) does not lead to an agreement with the results of Müller-Markgraf and Troe[8] in their earlier shock wave study at much higher temperatures. They obtained a rate constant k_1 = (6.6 ± 1.5) × $10^{-12}$$(T/1000\ K)^{+0.4}$ cm^3 $molecule^{-1}$ s^{-1} over the range 750 K ≤ *T* ≤ 950 K. Using eqn. (6), we expect a value of $k_1 = 2 \times 10^{-11}$ cm^3 $molecule^{-1}$ s^{-1} at 1600 K, a value ~3 times higher than that measured in ref. 8. It is unlikely that this disagreement is caused by uncertainties in $\sigma_{benzyl}(T)$ as a function of temperature: in ref. 8, $\sigma_{benzyl}(T) = 4 \times 10^{-17}$ cm^2 $molecule^{-1}$ was directly measured at (1160 ± 30) K and (1600 ± 20) K

Table 1 Pseudo-second-order rate constants for the combination reaction of benzyl radicals (k_1)

p (He)[a]	[He][b]	k_1[c]	p (He)[a]	[He][b]	k_1[c]	p (He)[a]	[He][b]	k_1[c]	p (He)[a]	[He][b]	k_1[c]
(a) M = He at 300 K											
25	5.97×10^{20}	4.60	80	1.86×10^{21}	5.05	100	2.31×10^{21}	4.85	150	3.39×10^{21}	5.23
40	9.48×10^{20}	3.59	90	2.09×10^{21}	4.88	120	2.74×10^{21}	4.41	200	4.42×10^{21}	5.06
60	1.41×10^{21}	4.76									
(b) M = Ar at 300 K											
p(Ar)[a]	[Ar][b]	k_1[c]	p(Ar)[a]	[Ar][b]	k_1[c]	p(Ar)[a]	[Ar][b]	k_1[c]	p(Ar)[a]	[Ar][b]	k_1[c]
0.03	1.17×10^{18}	4.60	8	1.93×10^{20}	5.13	90	2.17×10^{21}	6.10	692	1.24×10^{22}	3.22
0.05	1.65×10^{18}	3.67	10	2.41×10^{20}	4.67	100	2.53×10^{21}	5.99	756	1.29×10^{22}	2.92
0.07	2.23×10^{18}	4.06	12	2.90×10^{20}	4.57	120	3.04×10^{21}	5.85	788	1.32×10^{22}	3.58
0.09	3.58×10^{18}	4.11	15	3.62×10^{20}	4.43	158	4.01×10^{21}	5.87	841	1.35×10^{22}	2.96
0.15	4.83×10^{19}	4.03	25	6.04×10^{20}	5.31	220	5.53×10^{21}	4.90	842	1.36×10^{22}	2.96
2	7.24×10^{19}	4.97	40	9.66×10^{20}	5.30	318	7.61×10^{21}	3.93	864	1.37×10^{22}	3.96
3	9.66×10^{19}	4.50	50	1.21×10^{21}	5.92	408	9.16×10^{21}	3.56	850	1.36×10^{22}	3.50
4	1.45×10^{20}	5.42	60	1.45×10^{21}	5.92	507	1.05×10^{22}	3.37	900	1.39×10^{22}	3.56
6	1.93×10^{20}	4.61	80	1.93×10^{21}	4.56	597	1.15×10^{22}	3.14			
(c) M = N_2 at 300 K											
p(N_2)[a]	[N_2][b]	k_1[c]	p(N_2)[a]	[N_2][b]	k_1[c]	p(N_2)[a]	[N_2][b]	k_1[c]	p(N_2)[a]	[N_2][b]	k_1[c]
4	9.66×10^{19}	4.03	13	3.02×10^{20}	5.17	50	1.21×10^{21}	5.31	155	3.62×10^{21}	4.67
6	1.45×10^{20}	4.35	15	3.62×10^{20}	4.74	60	1.45×10^{21}	5.48	201	4.59×10^{21}	4.39
8	1.93×10^{20}	5.18	18	4.35×10^{20}	5.62	80	1.93×10^{21}	5.10			
10	2.41×10^{20}	5.11	40	9.66×10^{20}	5.17	117	2.79×10^{21}	5.38			
(d) M = CO_2 at 300 K											
p(CO_2)[a]	[CO_2][b]	k_1[c]	p(CO_2)[a]	[CO_2][b]	k_1[c]	p(CO_2)[a]	[CO_2][b]	k_1[c]	p(CO_2)[a]	[CO_2][b]	k_1[c]
0.04	9.61×10^{17}	4.17	0.45	1.08×10^{19}	3.96	12.00	3.08×10^{20}	6.03	30.00	8.67×10^{20}	8.26
0.07	1.71×10^{18}	3.79	3.00	7.35×10^{19}	4.51	15.00	3.92×10^{20}	6.39	31.60	9.25×10^{20}	7.07
0.10	2.36×10^{18}	4.09	4.00	9.85×10^{19}	4.76	18.00	4.79×10^{20}	7.33	35.00	1.05×10^{21}	9.29
0.20	4.85×10^{18}	4.11	6.00	1.49×10^{20}	4.84	20.00	5.39×10^{20}	7.74	41.60	1.33×10^{21}	8.73
0.30	7.24×10^{18}	3.67	8.00	2.01×10^{20}	5.52	21.60	5.89×10^{20}	6.61			
0.40	9.75×10^{18}	3.90	10.00	2.54×10^{20}	5.40	25.00	6.97×10^{20}	7.79			
(e) M = CO_2 at 275 K											
p(CO_2)[a]	[CO_2][b]	k_1[c]	p(CO_2)[a]	[CO_2][b]	k_1[c]	p(CO_2)[a]	[CO_2][b]	k_1[c]	p(CO_2)[a]	[CO_2][b]	k_1[c]
8	2.23×10^{20}	6.81	18	5.45×10^{20}	7.97	12	3.45×10^{20}	6.60	25	8.13×10^{20}	9.88
10	2.83×10^{20}	7.01	15	4.42×10^{20}	7.71	20	6.17×10^{20}	9.25	30	1.04×10^{21}	11.16
(f) M = CO_2 at 350 K											
p(CO_2)[a]	[CO_2][b]	k_1[c]	p(CO_2)[a]	[CO_2][b]	k_1[c]	p(CO_2)[a]	[CO_2][b]	k_1[c]	p(CO_2)[a]	[CO_2][b]	k_1[c]
2	4.16×10^{19}	3.83	6	1.26×10^{20}	4.28	12	2.57×10^{20}	5.26	20	4.40×10^{20}	5.64
3	6.26×10^{19}	4.00	8	1.69×10^{20}	4.79	15	3.25×10^{20}	5.05	25	5.59×10^{20}	5.60
4	8.37×10^{19}	4.52	10	2.13×10^{20}	4.65	18	3.93×10^{20}	5.51	30	6.83×10^{20}	5.80
(g) M = Ar: Xe (1:1 mixture) at 300 K											
p[a]	[M][b]	k_1[c]	p[a]	[M][b]	k_1[c]	p[a]	[M][b]	k_1[c]			
20	4.98×10^{20}	5.70	25	6.52×10^{20}	5.71	30	7.60×10^{20}	6.89			
(h) M = Ar: Xe (1:1 mixture) at 275 K											
p[a]	[M][b]	k_1[c]	p[a]	[M][b]	k_1[c]	p[a]	[M][b]	k_1[c]			
20	5.49×10^{20}	5.33	25	7.23×10^{20}	6.69	30	8.43×10^{20}	5.49			

[a] Pressure of the bath gas, given in bar. [b] Density of the bath gas, given in molecule cm^{-3}. [c] Rate constant, given in 10^{-11} cm^3 $molecule^{-1}$ s^{-1}.

following the thermal decomposition of several precursors (benzyl iodide, toluene, and ethyl benzene). This is comparable to $\sigma_{benzyl}(T = 1600\ K) = 3.4 \times 10^{-17}\ cm^2\ molecule^{-1}$, when one uses an estimated value recommended by Ikeda *et al.*[19] Therefore, a possible reason for this disagreement might be the derivation of k_1 from a complicated reaction system using benzyl iodide as a precursor, as done in ref. 8.

4.2. Theoretical analysis of $k_{1,\infty}^{ET}(T)$

In the preliminary report of the present results,[6] we have suggested that an analysis of $k_{1,\infty}^{ET}$, in terms of unimolecular rate theory is also of major importance for an analysis of the enhancement of k_1. In the following we, therefore, further elaborate the analysis of $k_{1,\infty}^{ET}(T)$. Unfortunately, sufficiently accurate *ab initio* potentials for reaction (1) are not yet available, a situation typical for systems involving large radicals. As a consequence we estimate $k_{1,\infty}^{ET}(T)$ on the basis of statistical adiabatic channel/classical trajectory (SACM/CT) calculations for a "standard" valence potential such as described in the articles by Maergoiz *et al.*[21,22] for a "linear + linear → non-linear" reaction with an adduct angle corresponding to that of dibenzyl. First, we calculate an upper limit of $k_{1,\infty}^{ET}$ given by phase space theory, $k_{1,\infty}^{ET,PST}$, which is determined by the interaction potential between the radicals neglecting the anisotropy. As usual, the long-range dipole–dipole potential in the present reaction is irrelevant because of the small dipole moment of benzyl radicals, which at the UHF level with a 6-31G(d,p) basis set[23] was calculated to be as small as 0.06 D.[24] Instead we characterized the interaction between two benzyl radicals by a

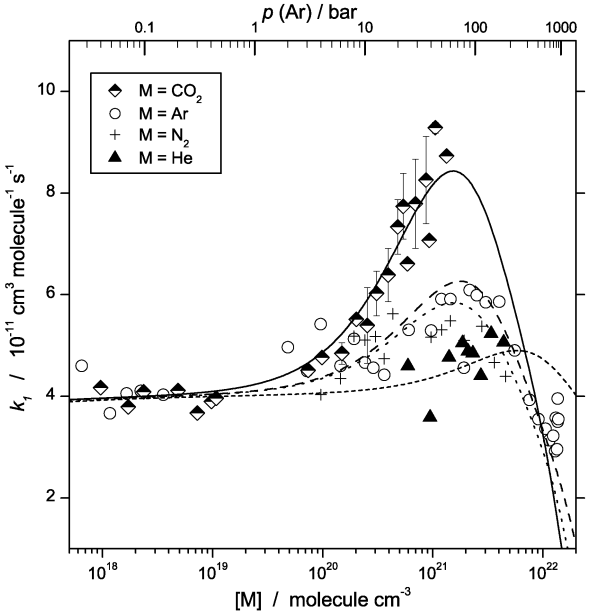

Fig. 3 Density dependence of the combination rate constant k_1 in helium (this work), argon, N_2 and CO_2 (ref. 7) at 300 K. Lines indicate the simulation from the kinetic model described in the text.

Morse potential. The capture rate constant from phase space theory is then expressed by:[21,22]

$$k_{1,\infty}^{\mathrm{ET,PST}} = \sqrt{\frac{8\pi kT}{\mu}}\frac{f}{\beta^2}\alpha_{\mathrm{spin}}Y(T) \qquad (7)$$

Here μ is the reduced mass of the two reactants; $\alpha_{\mathrm{spin}} = 1/4$ is the spin-statistical factor; the parameter f is equal to 0.5 for identical reactants; a reduced cross-section $Y(T) = -31.153 - 18.158X(T) + 0.8685X(T)^2 = 296.2$ is estimated[21,22] with $X(T) = \ln(kT/D_0) + 4 - \beta r_e = -9.9$. The equilibrium distance of the centre of mass of the two reactants in the adduct is $r_e = 5.5$ Å. The Morse parameter $\beta = 1.6$ Å^{-1} is estimated from the expression:[21,22]

$$\beta = 2\pi hc\nu_{\mathrm{C-C,str}}\sqrt{\frac{\mu_{\mathrm{C-C}}}{2D_0}} \qquad (8)$$

A value of the dissociation energy of $D_0/hc = 2.32 \times 10^4$ cm^{-1},[25] and a vibrational frequency in the C–C stretching mode, $\nu_{\mathrm{C-C,str}} = 976$ cm^{-1}, are used.[26] This leads to

$$k_{1,\infty}^{\mathrm{ET,PST}} = 1.7 \times 10^{-10}(T/300\ \mathrm{K})^{+0.40}\ \mathrm{cm^3\ molecule^{-1}\ s^{-1}} \qquad (9)$$

The comparison with the experimental results then gives an experimental rigidity factor of

$$f_{\mathrm{rigid}}^{\mathrm{exp}} \approx 0.24\ (T/300\ \mathrm{K})^{-0.5} \qquad (10)$$

One may also try to rationalize f_{rigid} by theory. In the absence of a higher quality potential energy surface, one cannot do much more than use the experimental $f_{\mathrm{rigid}}^{\mathrm{exp}}$ at 300 K and fit the ratio α/β of potential parameters which characterizes the anisotropy of the potential.[21,22] One then may calculate the temperature dependence of $f_{\mathrm{rigid}}^{\mathrm{theory}}$ and compare that with the corresponding experimental property of $f_{\mathrm{rigid}}^{\mathrm{exp}}$. Following the treatment of refs. 21 and 22, $f_{\mathrm{rigid}}^{\mathrm{exp}}(300\ \mathrm{K}) = 0.24$ is reproduced by $\alpha/\beta = 0.74$. Using this value, the theoretical calculation of $f_{\mathrm{rigid}}^{\mathrm{theory}}$ gives

$$f_{\mathrm{rigid}}^{\mathrm{theory}} \approx 0.24(T/300\ \mathrm{K})^{-0.6} \qquad (11)$$

in very good agreement with the experimental result from eqn. (10). Combining eqns. (9) and (11) gives

$$k_{1,\infty}^{\mathrm{ET,theory}}(T) = 4.1 \times 10^{-11}\ (T/300\ \mathrm{K})^{-0.23}\ \mathrm{cm^3\ molecule^{-1}\ s^{-1}} \qquad (12)$$

where the calculated temperature dependence agrees well with the experimental result from eqn. (6).

Table 2 Limiting "high-pressure" rate constants of the energy-transfer mechanism, $k_{1,\infty}^{\mathrm{ET}}(T)$

T/K	$\sigma_{\mathrm{benzyl}}(T)/10^{-16}$ cm^2 molecule^{-1}	$k_{1,\infty}^{\mathrm{ET}}(T)/10^{-11}$ cm^3 molecule^{-1} s^{-1}
250	1.34	5.03 ± 0.36
275	1.32	4.63 ± 0.50
300	1.30	4.10 ± 0.30
325	1.28	3.91 ± 0.21
350	1.25	3.32 ± 0.19
375	1.22	4.47 ± 0.55
400	1.20	3.13 ± 0.05

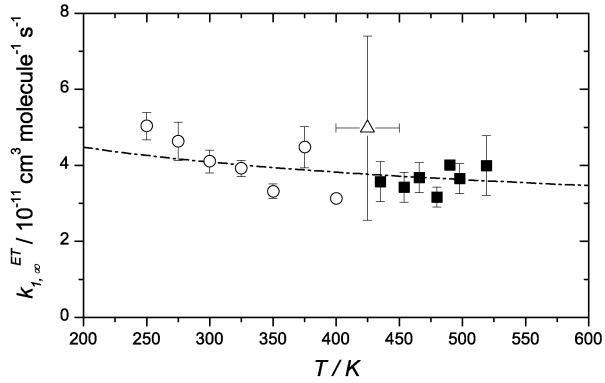

Fig. 4 Temperature dependence of $k_{1,\infty}^{\mathrm{ET}}(T)$: this study (O), ref. 9 (△), and ref. 10 (■). Data points of our study were measured and averaged over the pressure range of 1–5 bar in the bath gas argon (see Table 2). Data points of refs. 9 and 10 are corrected for $\sigma_{\mathrm{benzyl}}(T)$ (see text). The temperature dependence of the fitted line follows from SACM/CT calculations (see Section 4.2).

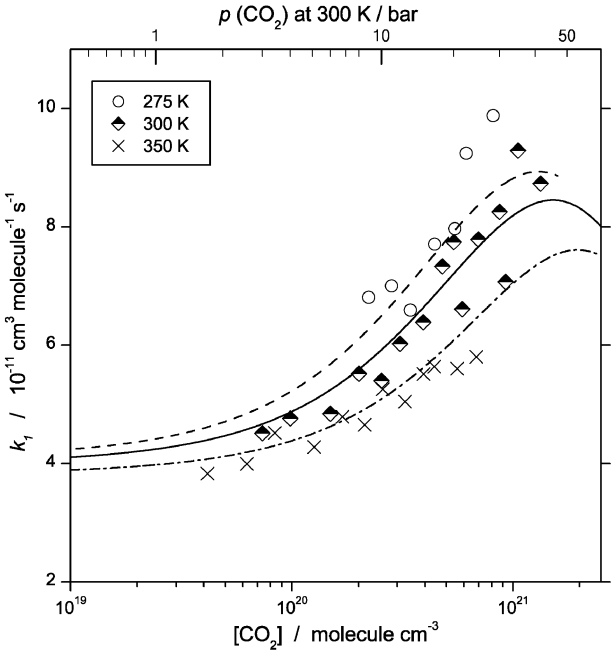

Fig. 5 Density dependence of the combination rate constant k_1 in CO_2 at different temperatures. Experimental data are from ref. 7, and lines are the results from a fit in terms of radical-complex mechanism (see text).

4.3. Transition to diffusion-controlled kinetics

At the highest pressure of Fig. 3, k_1 passes over a maximum and starts decreasing, which can be attributed to a transition to diffusion-controlled kinetics. Before analysing the intermediate zone of an enhancement of k_1, we now look at the high density range where the recombination is diffusion-controlled. Rate constants in the gas–liquid transition range traditionally have been approximated by a relationship:

$$k_{\mathrm{rec}} = k_{\mathrm{diff}}\left[\frac{k_{\mathrm{rec}}^{\mathrm{g}}}{k_{\mathrm{rec}}^{\mathrm{g}} + k_{\mathrm{diff}}}\right] \qquad (13)$$

with $k_{\mathrm{diff}} = 4\pi\alpha_{\mathrm{spin}}(M)RD$. Here k_{diff} is the value of k_1 in the range of diffusion control; $k_{\mathrm{rec}}^{\mathrm{g}}$ is the hypothetical value of the combination rate constant in the absence of diffusion control, *i.e.* the joint contribution from the energy-transfer mechanism (k^{ET}), the mechanism responsible for the enhancement of k_1 (k^{RC}); D is the diffusion coefficient of the recombining radicals in the bath gas; R is an effective capture distance; and $\alpha_{\mathrm{spin}}(M)$ denotes a possibly density-dependent electronic weight factor. At this stage we use α_{spin} of 1/4 for reaction (1). This relates to the simple picture that only one-fourth of the benzyl + benzyl encounters lead to singlet electronic ground-state bibenzyl, whereas three-fourths of the encounters are unsuccessful because they separate from an excited triplet state before they can attain the correct spin configuration (see ref. 6 for more detailed explanations). The contact distance R is usually taken as a more or less undefined fit parameter. Recently we suggested to relate R to the thermally averaged capture cross section $\langle\sigma\rangle$ of two radicals in the "high-pressure limit" within the energy-transfer mechanism:[6]

$$R = \sqrt{\frac{\langle\sigma\rangle}{\pi}} = \left(\frac{1}{\alpha_{\mathrm{spin}}(M)\pi f}k_{\infty}^{\mathrm{ET}}\sqrt{\frac{\pi\mu}{8kT}}\right)^{1/2} \qquad (14)$$

where f is 1/2 for identical reactants and μ is the reduced mass of the two radicals. Following this suggestion, one derives R = 5.3 Å. It is interesting to note that a similar value (R = 5.9 Å) was estimated by Claridge and Fischer[11] in their kinetic studies of the self-termination of benzyl radicals in liquid cyclohexane, averaging the results from three methods: (a) from the molar volume of the corresponding toluene and a space filling factor for cubic close packing, (b) from a simple volume increment method, and (c) from a volume increment method using LeBas increments.

Experimental measurements of tracer diffusion coefficients for radicals in liquids or supercritical fluids are rare. Fortunately there have been efforts to measure D for benzyl radicals in liquids.[27–31] By using the photochemical space intermittency (PCSI) method, Burkhart *et al.*[28–30] measured D of benzyl radicals in cyclohexane and determined $D_{\mathrm{benzyl}} = 1.1 \times 10^{-5}$ cm^2 molecule^{-1} s^{-1}. More recently, Terazima *et al.*[27] applied the time-resolved transient grating method and obtained $D_{\mathrm{benzyl}} = 4.1 \times 10^{-5}$, 0.95×10^{-5}, 1.1×10^{-5}, 0.64×10^{-5} cm^2 molecule^{-1} s^{-1} in hexane, cyclohexane, ethanol and 2-propanol, respectively. In Fig. 6, these literature values are plotted as a function of the inverse viscosity of the studied liquid solvents. There is, however, no direct measurement of D_{benzyl} in the medium density region of our experiments, such that we cannot directly use the mentioned experimental results to our high-pressure data. In order to overcome this problem, we calculated density-dependent diffusion coefficients of toluene, because, at least in liquids, D_{benzyl} is known to be very close to the value of D of toluene.[27] Assuming that the ratio $D_{\mathrm{benzyl}}/D_{\mathrm{toluene}}$ is independent of the density in the medium density region, we determined density-dependent values of D_{benzyl} on the basis of calculated D_{toluene}. Fortunately, several currently available semi-empirical calculations of tracer diffusion in supercritical fluids have used toluene as a model. We used the semi-empirical method suggested in refs. 32 and 33.

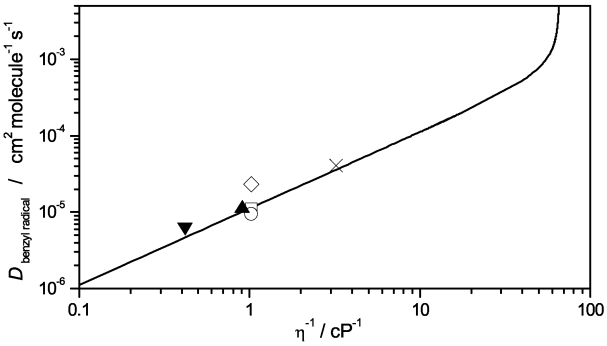

Fig. 6 Diffusion coefficients of benzyl radicals in liquid solvent media as a function of the inverse of the viscosity of the liquid; in 2-propanol (▼, ref. 27), in ethanol (▲, ref. 27), in cyclohexane (○, ref. 27, □, ref. 28, and ◇, ref. 11), and in hexane (×, ref. 27). The solid line represents the calculated values for D_{benzyl} in this work (see text).

This approach is based on the rough hard sphere theory which treats the intermolecular interaction between solute and solvent as being of Lennard-Jones (LJ) type. The result assuming $D_{\mathrm{benzyl}} \approx D_{\mathrm{toluene}}$ is plotted in Fig. 6 as a function of the inverse viscosity of the bath gas CO_2. The extrapolation of the derived D_{benzyl} to the liquid densities shows good agreement with the literature data in various liquid solvents mentioned above, which suggests the quality of the derived D_{benzyl}.

Figs. 7 and 8 employs the calculated rate constants k_{diff}, k_1 from the energy-transfer range, and eqn. (13) for a separate identification of that part of k_1 (denoted by k^{RC}) which is responsible for the enhancement of k_1 at intermediate densities. Diffusion control in the high-density region is clearly limiting the kinetics at the highest pressures. We note that in our work it was not necessary to employ any fit parameters to specify k_{diff} in eqn. (13).

4.4. Contribution k^{RC} from the radical-complex mechanism

Our experimental data for k_1 at pressures of about 10–300 bar in the bath gas argon and of about 3–50 bar in CO_2, clearly differ from a smooth transition between energy-transfer and

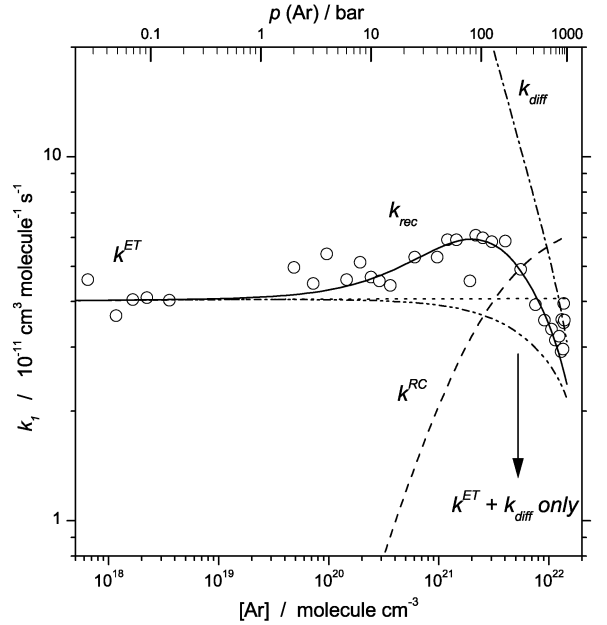

Fig. 7 Density dependence of the combination rate constant k_1 in the bath gas argon (○) at 300 K. (···): k^{ET} from the energy-transfer mechanism; (–•–): limiting diffusion-controlled rate constants; (– – –): k^{RC} from the radical-complex mechanism; (–••–): resulting rate constants without k^{RC}; and (——):resulting rate constants including k^{RC}. Fitting parameters used in this calculation are summarised in Table 2.

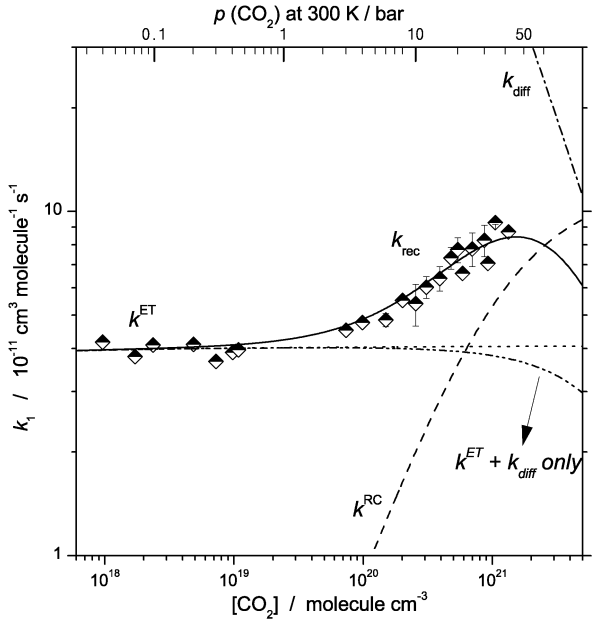

Fig. 8 As Fig. 7, at 300 K in CO_2 (half-filled diamonds).

diffusion-controlled kinetics (see the dashed–dot–dot line, "k^{ET} + k_{diff} *only*" in Figs. 7 and 8, respectively). We have made a similar observation in the combination of CCl_3 radicals with Br and CCl_3.[6] However, the effect is much more easily observed in the present case because the energy-transfer mechanism of the recombination is already in the "high-pressure limit" over the pressure range 0.1–1 bar. The enhancement of k_1, therefore, can be identified and quantified much better. The additional contribution k^{RC} to k_1 shown in Figs. 7 and 8 is the central and new piece of information derived in this work. We tentatively as before attribute it to a radical-complex mechanism. In the following we try to provide a quantitative interpretation of k^{RC} within this mechanism.

Analogous to ref. 6, we assume that benzyl radical combination involves an energy-transfer, eqn. (15), and a radical-complex, eqn. (16), contribution:

$$\begin{aligned} &A + A \leftrightarrows A_2^* \quad k_a, k_{-a} \\ &A_2^* + M \rightarrow A_2 + M \quad k_b \end{aligned} \tag{15}$$

$$\begin{aligned} &A + M \leftrightarrows AM \quad k_c, k_{-c}, K_{eq} \\ &AM + A \rightarrow A_2 + M \quad k_{AM+A} \\ &AM + AM \rightarrow A_2 + 2M \quad k_{AM+AM} \end{aligned} \tag{16}$$

Here A denotes the benzyl radical and M is the bath gas. Neglecting diffusion control, the combined rate constant from both mechanisms is represented by

$$k_{1,rec} = k_1^{ET} + k_1^{RC} = \frac{k_{1,\infty}^{ET} k_{1,0}^{ET}[M]}{k_{1,\infty}^{ET} + k_{1,0}^{ET}[M]} F_c + \frac{K_{eq} k_{AM+A}[M] + K_{eq}^2 k_{AM+AM}[M]^2}{(1 + K_{eq}[M])^2} \tag{17}$$

k_1^{ET} is characterized by the limiting low- and high-pressure rate constants $k_{1,0}^{ET}$ and $k_{1,\infty}^{ET}$, respectively, and a broadening factor of the falloff curve. The equilibrium constant K_{eq} contained in k_1^{RC} was estimated following refs. 6 and 34, using Lennard-Jones parameters of $\sigma_{LJ} = 5.92$ Å and $\varepsilon_{LJ} = 410$ K for benzyl radicals such as given by the values of toluene. The values of K_{eq} at 300 K for different bath gases are summarised in Table 3; they are in the range 0.6–11 $\times 10^{-22}$ cm^3 molecule^{-1} and show an increasing order $K_{eq}(He) < K_{eq}(N_2) \approx K_{eq}(Ar) < K_{eq}(CO_2)$. k_{AM+A} controls the onset while k_{AM+AM} describes

Table 3 Contribution to k^{RC} for the radical-complex mechanism

M	T/K	K_{eq}(AM)[a]	k_{AM+A}[b]	k_{AM+AM}[b]
He	300	6.6×10^{-23}	8.08×10^{-11}	5.64×10^{-11}
N_2	300	4.9×10^{-22}	8.36×10^{-11}	7.22×10^{-11}
Ar	300	5.8×10^{-22}	8.36×10^{-11}	7.52×10^{-11}
CO_2	300	1.1×10^{-21}	8.85×10^{-11}	1.19×10^{-10}
CO_2	275	1.4×10^{-21}	8.95×10^{-11}	1.20×10^{-10}
CO_2	350	6.7×10^{-22}	8.67×10^{-11}	1.17×10^{-10}

[a] Equilibrium constant, given in cm^3 molecule^{-1}, [b] Rate constant, given in cm^3 molecule^{-1} s^{-1}.

the "high-pressure limit" of the rate constant in the radical-complex mechanism. k_{AM+A} and k_{AM+AM} can both be fitted independently, see Figs. 7 and 8. The solid lines account for contributions from the usual energy-transfer mechanism and from the radical-complex mechanism. As compared with the dashed–dot–dot lines ("$k_{1,\infty}^{ET}$ + k_{diff} *only*"), the addition of a radical-complex component results in a much better representation of the experimental data. Similar fits were applied to the N_2 and helium data, and the results are summarized in Table 3 and plotted in Fig. 3. The fits of the experiments (see Table 3) suggest that values of k_{AM+A} and k_{AM+AM} for A = benzyl and M = bath gas are always larger than k_{A+A} (= $k_{1,\infty}^{ET}$) and increase in the order $k_{A+A} < k_{AM+A} < k_{AM+AM}$. k_{AM+A} and k_{AM+AM}, on the other hand, increase in the order He < N_2 ≈ Ar < CO_2.

If k_{AM+A} and k_{AM+AM} would not be larger than k_{A+A}, then no rate constant enhancement of k_1 would have been observed. It is, therefore, of central importance to rationalize the conclusion about the order of the rate constants, *i.e.* $k_{A+A} < k_{AM+A} < k_{AM+AM}$. Simple phase space theory does not explain the observed trend. Actually, by the methods described in Section 4.2, we obtained values of $k_{AM+AM}^{PST} \approx k_{A+A}^{PST} = 1.7 \times 10^{-10}$ cm^3 molecule^{-1} s^{-1}, because the effects of different cross sections and reduced masses partially compensate. In this calculation, the distance of the center of mass of the two reactants, r_e, was estimated as $r_{e,AM+AM} = 6.8$ Å and $r_{e,A+A} = 5.5$ Å following structural optimisation on the UB3LYP level with a 6-31G(d,p) basis set.[23] In addition, we assumed that the dissociation energies $D_{0,A+A} \approx D_{0,AM+AM} = 2.32 \times 10^4$ hc cm^{-1},[25] and that the change in the vibrational frequencies in the C–C stretching modes, $\nu_{C-C,str}$, for A + A and AM + AM, are negligible.

If the phase space limits of the rate constants are equal, the differences between k_{AM+AM} and k_{A+A} can only be found in different rigidity factors. In ref. 6 we suggested that the presence of a van der Waals complex partner M may shield and reduce the anisotropy of the valence potential between A and A which then results in larger rigidity factors.[6] f_{rigid}^{exp} in k_{AM+AM} was found to increase in the order He (≈0.33) < N_2 (≈0.43) ≈ Ar (≈0.45) < CO_2 (≈0.70). It appears important to note that f_{rigid}^{exp} is still below unity. It appears also of interest to mention that a similarly high rigidity factor as in the bath gas of CO_2 was also observed in our subsequent studies of benzyl combination in the bath gases CF_3H or SF_6.[35] f_{rigid}^{exp} in k_{AM+A} only showed small variations but was still increasing in the order He (≈0.25) < N_2 (≈0.26) ≈ Ar (≈0.26) < CO_2 (≈0.27). It was found to be between the values of f_{rigid}^{exp} in k_{AM+AM} and f_{rigid}^{exp} in k_{A+A} (= 0.24). In summary, our interpretation in terms of the different rigidity factor appears consistent with the experimental observations. At present these interpretations still have some hypothetical character and need further back up from quantitative tests in other experimental systems and from detailed CT calculations of the capture process on improved potential surfaces. Both are underway and a corresponding comprehensive treatment will be given in the future. However the present study already provides another piece of experimental evidence for the assumed role of the

radical-complex mechanism: A pronounced negative temperature dependence of the rate constant enhancement at the elevated densities was observed, just in line with basic expectations for increasing contributions from radical-complex mechanism at decreasing temperatures. This is discussed in the following section.

4.5. Temperature dependence of the radical-complex mechanism

For a further test, we also investigated the temperature dependence of the rate constant enhancement in the medium density region. To our knowledge, a quantitative analysis of this effect is reported here for the first time. Fig. 5 shows a fit to our experimental data in the bath gas CO_2 at the temperatures 275 K, 300 K and 350 K (see Table 3 for the fitted values). The observation of a larger enhancement at lower temperatures supports our hypothesis of a contribution from the radical-complex mechanism. Both the equilibrium constants $K_{eq}(T)$ and the rate constants $k_{AM+A}(T)$ and $k_{AM+AM}(T)$ are expected to depend on the temperature.

First, we consider $K_{eq}(T)$. The temperature dependence of $K_{eq}(T)$ was estimated following the method described in refs. 6 and 34, and the resulting values are summarized in Table 3. Over the temperature range 250–400 K, they can be represented as

$$K_{eq}(T) = 1.1 \times 10^{-21}\ (T/300\ \mathrm{K})^{-3}\ \mathrm{cm^3\ molecule^{-1}} \quad (18)$$

Second, we derived expressions for the rate constants of $k^{exp}_{AM+AM}(T)$ and $k^{exp}_{AM+A}(T)$ from the experiments, see Table 3. We obtained

$$k^{exp}_{AM+AM}(T) = 1.2\times10^{-10}(T/300\ \mathrm{K})^{-0.1}\ \mathrm{cm^3\ molecule^{-1}\ s^{-1}} \quad (19)$$

and

$$k^{exp}_{AM+A}(T) = 8.8\times10^{-11}(T/300\ \mathrm{K})^{-0.1}\ \mathrm{cm^3\ molecule^{-1}\ s^{-1}}. \quad (20)$$

It should be noted that the slightly negative temperature coefficients of $k^{exp}_{AM+AM}(T)$ and $k^{exp}_{AM+A}(T)$ are similar to those obtained for $k^{exp}_{A+A}(T)$ in eqn. (6). Third, temperature-dependent rigidity factors of

$$f^{exp}_{rigid,AM+AM}(T) = 0.70\ (T/300\ \mathrm{K})^{-0.5} \quad (21)$$

and

$$f^{exp}_{rigid,AM+A}(T) = 0.27\ (T/300\ \mathrm{K})^{-0.5} \quad (22)$$

were derived from the experiments. These results of $k^{exp}_{AM+AM}(T)$ and $f^{exp}_{rigid,AM+AM}(T)$ were then compared with theoretical estimates such as described in Section 4.2. Briefly, we characterised the interaction between two AM (benzyl + CO_2) by a Morse potential with $r_{e,AM+AM} = 6.8$ Å and we fitted $\alpha/\beta \approx 0.77$ from the value of f_{rigid} at 300 K.[21] Following the method as described before, we predicted

$$f^{theory}_{rigid,AM+AM} \approx 0.70\ (T/300\ \mathrm{K})^{-0.4} \quad (23)$$

which is very close to our experimental temperature dependence of $f^{exp}_{rigid,AM+AM}$ in eqn. (21). In total, we obtained a theoretical estimate of

$$k^{theory}_{AM+AM}(T) = 1.2 \times 10^{-10}\ (T/300\ \mathrm{K})^{-0.05}\ \mathrm{cm^3\ molecule^{-1}\ s^{-1}} \quad (24)$$

which is again in agreement with the experimental result from eqn. (19). Fig. 9(a and b) illustrates the derived rate constants k_{AM+AM} (T), k_{A+A} (T) and $k^{PST}(T)$ as well as the temperature-dependent rigidity factors for the AM + AM and A + A reactions. The results provide an internally consistent interpretation in terms of the radical-complex mechanism.

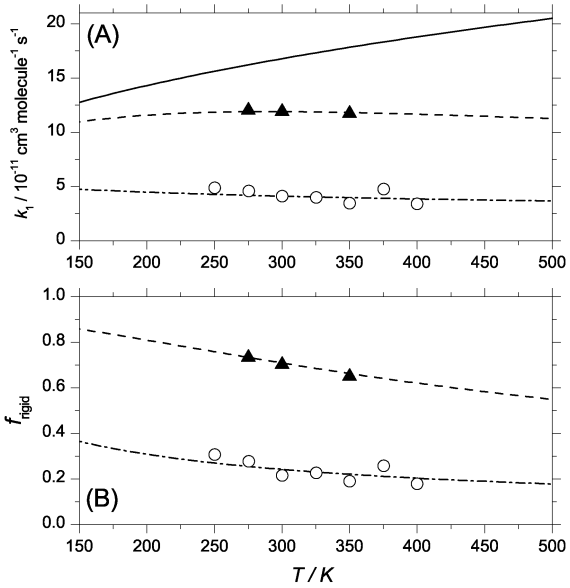

Fig. 9 (A) Temperature dependence of thermal capture rate constants of benzyl radicals in the bath gas CO_2. (——): $k^{PST}(T)$; (--): k_{AM+AM} (T); and (–•–): $k_{A+A}(T)$. Experimental data are: (▲) $k^{exp}_{AM+AM}(T)$ at temperatures of 275, 300, and 350 K in the CO_2 bath gas, (○) $k_{A+A}{}^{exp}$(T) (= $k^{ET}_{1,\infty}(T)$) in the argon bath gas from Fig. 4. (B) Temperature dependence of calculated thermal rigidity factors for reaction (1) in the bath gas CO_2. (--): $f^{theory}_{rigid,AM+AM}(T)$; and (–•–): $f^{theory}_{rigid,A+A}(T)$. Experimental data are: (▲): $f^{exp}_{rigid,AM+AM}(T)$; and (○): $f^{exp}_{rigid,A+A}(T)$.

5. Conclusions

The combination reaction $C_6H_5CH_2 + C_6H_5CH_2$ (+M) → $C_{14}H_{14}$ (+M) was studied at temperatures of 250–400 K over the pressure range 0.03–900 bar in the bath gases helium, argon, xenon, N_2 and CO_2. The fact that the reaction rate constants reach a pressure-independent range at pressures as low as 0.01 bar, allowed us to determine the limiting "high-pressure" rate constant of the energy-transfer mechanism $k^{ET}_{1,\infty}$ without doing falloff extrapolation. $k^{ET}_{1,\infty}$ could be determined as

$$k^{ET}_{1,\infty}(T) = (4.1 \pm 0.3) \times 10^{-11}\ (T/300\ \mathrm{K})^{-0.23}\ \mathrm{cm^3\ molecule^{-1}\ s^{-1}}$$

This value was analysed in terms of SACM/CT theory. The observed increase of the rate constants at higher pressures, between about 5 bar and the onset of diffusion-limited kinetics above about 50 bar, was interpreted in terms of a radical-complex mechanism. A quantitative analysis of absolute values and temperature dependences of rate constants in the range of the radical-complex mechanism was given. A proof of the suggested mechanism and more quantitative conclusions requires *ab initio* information on the potential between uncomplexed and complexed radicals. As long as this information is not available, the given interpretation remains tentative. In particular, the possibility of collision-induced electronic transitions, which could convert triplet benzyl pairs into singlets, cannot be ruled out. We did not discuss this possibility in the present article. An empirical investigation of this point will be described in the future when more experimental data for more diverse systems will have been collected. For the moment, however, the hypothesis of a contribution of the radical-complex mechanism in the pressure range between about 5 and 50 bar could be supported by an intrinsically consistent quantitative analysis. If the present interpretation is correct, one has to expect similar phenomena quite generally in radical–radical recombination reactions.

Acknowledgements

Financial support by the Alexander von Humboldt Foundation (“Sofja Kovalevskaja Program”) and the Deutsche Forschungsgemeinschaft (Sonderforschungsbereich 357 “Molekulare Mechanismen unimolekularer Prozesse”) is gratefully acknowledged. Discussions with V. G. Ushakov, T. Lenzer, D. A. Wild, J. Schroeder, D. Schwarzer and M. Teubner were also most helpful.

References

1 Y. Arai, T. Sako and Y. Takebayashi, *Supercritical Fluids-Molecular Interactions, Physical Properties, and New Applications*, Springer-Verlag, Berlin, Heidelberg, 2002.
2 T. Clifford, *Fundamentals of Supercritical Fluids*, Oxford University Press, New York, 1999.
3 Y. P. Sun, *Supercritical Fluid Technology in Materials Science and Engineering*, Marcel Dekker, Inc., NewYork, 2002.
4 J. Troe, *J. Phys. Chem.*, 1986, **90**, 357.
5 B. Otto, J. Schroeder and J. Troe, *J. Chem. Phys.*, 1984, **81**, 202.
6 K. Oum, K. Luther and J. Troe, *J. Phys. Chem. A.*, 2004, **108**, 2690.
7 K. Oum, K. Sekiguchi, K. Luther and J. Troe, *Phys. Chem. Chem. Phys.*, 2003, **5**, 2931.
8 W. Müller-Markgraf and J. Troe, *J. Phys. Chem.*, 1988, **92**, 4899.
9 F. F. Fenter, B. Noziere, F. Caralp and R. Lesclaux, *Int. J. Chem. Kinet.*, 1994, **26**, 171.
10 A. Boyd, B. Noziere and R. Lesclaux, *J. Phys. Chem.*, 1995, **99**, 10815.
11 R. F. Claridge and H. Fischer, *J. Phys. Chem.*, 1983, **87**, 1960.
12 C. B. Roberts, J. Zhang, J. F. Brennecke and J. E. Chateauneuf, *J. Phys. Chem.*, 1993, **97**, 5618.
13 H. Stark, PhD Thesis, Göttingen University, 1999.
14 K. Luther, K. Oum and J. Troe, *J. Phys. Chem. A.*, 2001, **105**, 5535.
15 J. Hahn, K. Luther and J. Troe, *Phys. Chem. Chem. Phys.*, 2000, **2**, 5098.
16 N. Fay, PhD Thesis, Göttingen University, 1997.
17 B. Noziere, R. Lesclaux, M. D. Hurley, M. A. Dearth and T. J. Wallington, *J. Phys. Chem.*, 1994, **98**, 2864.
18 H. Perkampus, *UV-VIS Atlas of Organic Compounds*, VCH: Weinheim, 1992.
19 N. Ikeda, N. Nakashima and K. Yoshihara, *J. Phys. Chem.*, 1984, **88**, 5803.
20 F. Markert and P. Pagsberg, *Chem. Phys. Lett.*, 1993, **209**, 445.
21 A. I. Maergoiz, E. E. Nikitin, J. Troe and V. G. Ushakov, *J. Chem. Phys.*, 1998, **108**, 5265.
22 A. I. Maergoiz, E. E. Nikitin, J. Troe and V. G. Ushakov, *J. Chem. Phys.*, 1998, **108**, 9987.
23 M. J. Frisch, G. W. Trucks, H. B. Schlegel, P. M. W. Gill, B. G. Johnson, M. A. Robb, J. R. Cheeseman, T. Keith, G. A. Petersson, J. A. Montgomery, K. Raghavachari, M. A. Al-Laham, V. G. Zakrzewski, J. V. Ortiz, J. B. Foresman, J. Cioslowski, B. B. Stefanov, A. Nanayakkara, M. Challacombe, C. Y. Peng, P. Y. Ayala, W. Chen, M. W. Wong, J. L. Andres, J. S. Binkley, D. J. Defrees, J. Baker, J. P. Stewart, M. Head-Gordon, C. Gonzalez and J. A. Pople, *Gaussian 98, revision A.7.*, Gaussian, Inc., Pittsburgh, PA, 1998.
24 D. A. Wild and T. Lenzer, private communication.
25 H. Hippler and J. Troe, *J.Phys. Chem.*, 1990, **94**, 3803.
26 T. Lenzer, D. A. Wild, K. Oum, K. Luther and J. Troe, in preparation.
27 K. Okamoto, N. Hirota and M. Terazima, *J. Phys. Chem. A.*, 1997, **101**, 5269.
28 R. D. Burkhart, *J. Phys. Chem.*, 1969, **73**, 2703.
29 R. D. Burkhart, R. F. Boynton and J. C. Merrill, *J. Am. Chem. Soc.*, 1971, **93**, 5013.
30 R. D. Burkhart and R. J. Wong, *J. Am. Chem. Soc.*, 1973, **95**, 7203.
31 M. Terazima, *Acc. Chem. Res.*, 2000, **33**, 687.
32 E. Ruckenstein and H. Liu, *Ind. Eng. Chem. Res.*, 1997, **36**, 3927.
33 H. Liu and E. Ruckenstein, *Ind. Eng. Chem. Res.*, 1997, **36**, 5488.
34 D. Schwarzer and M. Teubner, *J. Chem. Phys.*, 2002, **116**, 5680.
35 C. Y. Lee, K. Luther, K. Oum, K. Sekiguchi and J. Troe, in preparation.